RESEARCH PAPER

Sol-Gel Synthesis of MgO/CNT Nanocomposites: Structural, Optical, and Antibacterial Properties

Huda T. Abbas *, Mohammad Merdan, Hikmat A. Banimuslem

Department of Physics, College of Science, University of Babylon, Babylon, Iraq

ARTICLE INFO

Article History:
Received 11 October 2025
Accepted 20 February 2026
Published 01 April 2026

Keywords:
Antibacterial activity
Carbon nanotubes
MgO Nanoparticles
Sol-gel method

ABSTRACT

Magnesium oxide (MgO)/carbon nanotube (CNT) nanocomposites were prepared in this study through sol-gel process method. The use of CNT, known for its unique electrical, mechanical, and thermal properties, had a profound effect on the structural, optical, and antibacterial properties of the composites. UV–Vis studies showed a non-linear decrease in the direct band gap from 4.05 eV for pure MgO to 3.86 eV at 3% CNT at the optimal peak position, 3.94 eV at 2% CNT, caused by the minimal particle accumulation and the good CNT dispersion. Field emission scanning electron microscopy (FESEM) revealed that the greatest variation in particle size and distribution occurred as the CNT doping increased, and the most homogeneous structure was obtained at 2 % CNT. Bacterial tests revealed that the activity of MgO/CNTs against Gram-positive S. and Gram-negative S. was stronger. The 3% CNT composite containing synergistic antimicrobial action properties gave the highest zones of inhibition. These results highlight the promising applications of MgO/CNT nanocomposites prepared sol-gel method for nano-optoelectronics, nanomedicine, and environmental disinfection.

How to cite this article
Abbas H., Merdan M., Banimuslem H. Sol-Gel Synthesis of MgO/CNT Nanocomposites: Structural, Optical, and Antibacterial Properties. J Nanostruct, 2026; 16(2):2616-2628. DOI: 10.22052/JNS.2026.02.100

INTRODUCTION

Nanoparticles (NPs) have attracted much interest in the past few decades due to their unique physical and chemical properties, such as high strength accompanied by excellent thermal conductivity, improved damping capacities, and mechanical stability [1-7]. Metal oxide nanoparticles are an important type of nanomaterial and have been widely applied in biosensing technology, tissue engineering, catalysis, food packaging, biomedicine, and environmental science [8-11].

Magnesium oxide nanoparticle (MgO NPs) is one of the inorganic compounds well known for its unique properties such as white color, crystal structure with a high melting point of 2852°C, thermal resistance, chemical stability in environmental conditions, and good absorbent of heat. It is through which it also exhibits greater potential for being used as a thermal barrier material [12-14], which can also be used in many areas. MgO is also employed in the manufacture of industrial furnaces and stoves, in cement production, and within the medical sphere as an antacid and a laxative. In the nano-size state, MgO has a high reactivity, possessing a great surface area, and can be used for advanced applications including water purification, energy storage, and the development of nano sensors. These properties

* *Corresponding Author Email: hoda.hashem689@student.uobabylon.edu.iq*

This work is licensed under the Creative Commons Attribution 4.0 International License.
To view a copy of this license, visit http://creativecommons.org/licenses/by/4.0/.

augment the efficiency of environmental and biochemical processes and further enhance their scientific and practical applications [15-17]. Carbon nanotubes (CNT) are a kind of nano-material with a unique structure and excellent performance, which has won extensive attention in the field of scientific research [18,19]. These nanotubes are tubular, hollow, rolled-up graphene sheets that can be classified primarily into two types: single-walled carbon nanotubes (SWCNTs) and multi-walled carbon nanotubes (MWCNTs) according to the number of graphene layers [20,21].

CNTs possess excellent, unique physical and chemical properties such as high electrical conductivity, extraordinary mechanical strength, huge surface area, and good thermal stability and chemical inertness. These properties are strongly dependent on the synthesis conditions and the catalyst type, which were used during preparation [22,23].

These unique features enable the use of CNT in a broader range of advanced applications, such as the field of nanoelectronics, biosensor technology, and energy storage and conversion (e.g., batteries and solar cells) [24]. They are also used as fillers in composite materials such as concrete, rubber, and polystyrene. Furthermore, CNTs have immense potential applications in the medical field, particularly in targeted drug delivery, and also in environmental and water treatment technologies [24-26]. Nanoparticles based on metal oxide (MO-NPs) are potent antibacterial agents owing to their high surface area and the reactive oxygen species (ROS) that they can generate, damaging bacterial surfaces, proteins, and DNA [27,28]. The thermal stability, low toxicity, and powerful antibacterial performance of MgO NPs against Gram-positive and negative bacteria are the unique features of MgO NPs. This is primarily due to the generation of superoxide ions, resulting in damage to the bacterial cell architecture [29].

The blending between MgO NPs and CNTs can greatly enhance the antimicrobial properties. CNTs promote the dispersion of MgO NPs, inhibit aggregation, and increase the surface contact with bacteria. Such nanocomposites have strong antibacterial activity and are applicable in the medical and environmental as their compatibility and antibiotic resistance. Nanoparticles can be manufactured by a variety of techniques, including chemical vapor deposition (CVD), plasma-enhanced chemical vapor deposition (PECVD), pulsed laser deposition (PLD), laser ablation, molecular beam epitaxy (MBE), sputtering, hydrothermal routes, sol-gel processes, and co-precipitation [30]. One of the useful methods to produce large quantities of MgO nanoparticles is the sol-gel process, where a liquid solution is turned into a solid gel. This method is simple and efficient, producing high-purity NPs with excellent magnetic and optical properties. It also requires low temperature and provides better composition control over metal oxides, which makes it suitable for academic and industrial applications. Moreover, the nanoparticles prepared by this approach with specific properties, such as high surface area, small pore size, and small particle size, can increase their usefulness in killing the bacteria [31-33]. Bacteria are single-celled organisms that can be helpful as well as morbid. Although some of them are essential for maintaining the circle of life, pathogenic bacteria are responsible for life-threatening infections in human health and agriculture due to their ability to adapt and resist antibiotics [34]. Accordingly, this study aims to synthesize a MgO/CNT nanocomposite using the sol–gel technique at room temperature and evaluate its antibacterial activity against *Streptococcus* and *Serratia* pathogenic strains, thereby contributing to exploring its potential in biomedical and environmental applications.

MATERIALS AND METHODS

Synthesis of MgO Nanoparticles Incorporating Carbon Nanotubes

Magnesium oxide (MgO) nanoparticles were synthesized using the sol-gel method, as follows: A 0.1 M solution of magnesium nitrate $Mg(NO_3)_2{\cdot}6H_2O$ was prepared by mixing 10.25 g of magnesium nitrate with 400 ml of deionised water and stirred continuously. The pH of the solution was incrementally increased to 8.5 by the slow addition of a 25% ammonia solution, introduced dropwise every five minutes to ensure pH stability during the process. The mixture was subsequently positioned on a heating plate with a magnetic stirrer at 80°C and agitated at moderate speed for one hour, resulting in the production of a gel of magnesium hydroxide ($Mg(OH)_2$). The gel was allowed to cool to room temperature and then filtered and washed several times with deionised water to remove leftover ions and impurities. The resultant solid was subjected to drying in an oven at 100°C overnight, followed by calcination

CC BY

at 500°C for 2.2 hours at a programmable furnace with 10 °C heating and cooling rate to get the final MgO NPs.

After getting pure MgO, a nanocomposite of MgO with CNT has been prepared. Different percentages (0.1, 0.5, 1, 2, and 3 wt%) of CNT to MgO were conducted by dispersing 0.001, 0.005, 0.01, 0.02, and 0.03 g of carbon nanotubes in deionized water and sonicated for 30 minutes. The dispersion was then added dropwise to another solution of MgO previously placed on a magnetic stirrer. We subsequently positioned the resultant solution on a heating plate with a magnetic stirrer at 80°C for one hour to facilitate gel formation. The resulting gel, mainly made of MgO mixed evenly with CNT, Thereafter, the resultant gel was then allowed to cool to room temperature, filtered, and thoroughly washed more than five times with deionised water to remove ions and leftover impurities. The resultant solid was dried in an oven at 100°C for an entire night to produce the final MgO nanoparticles supported by CNT. A different method was used to create the MgO–CNT composite, where CNT were mixed with MgO NPs and then heated to 500 °C. However, later tests showed that the CNT broke down at high temperatures, leaving only pure magnesium oxide in the final product. Subsequent characterisations, however, indicated that the CNT disintegrated at elevated temperatures, resulting in the final product consisting solely of pure MgO. Consequently, we employed the aforementioned sol-gel process to maintain the presence of CNT in the final composite structure. This method involved dispersing CNT in the precursor solution before gel formation and drying without calcination; hence, it prevented thermal degradation. After drying, the powder was ground mechanically for a while to get homogeneous and fine NPs of the MgO/CNT composite.

RESULTS AND DISCUSSION

Structural properties

The structural properties of MgO and its composites doped with CNT at different concentrations (0.1%, 0.5%, 1%, 2%, and 3%) were probed using X-ray diffraction (XRD). The crystallite size was calculated using the Debye–Scherrer equation (see Eq. (1)). The typical diffraction peaks representing the (111), (200), (220), (311), and (222) crystal planes were observed in the pure MgO sample at the 2θ of 38.0°, 43.9°, 63.3°, 75.6°, and 79.5°, respectively, As shown in the Figs. 1 and 2. These peaks validate the presence of the face-centred cubic (FCC) structure of MgO, which is characteristic of MgO and reports high crystallinity and formation of a cubic phase in the MgO NPs [35].

The prepared sample's average crystal size (D) is 12.2 nm, with a corresponding lattice parameter (a) of 4.1 Å. These values align well with typical reports in the literature for nanostructured MgO [36]. The parameters were determined using the Scherrer method and verified through Williamson–Hall analyses in similar systems.

$$D = \frac{K\lambda}{\beta . \cos\theta} \quad (1)$$

where: D is the crystallite size. K is a numerical factor frequently called the crystallite-shape factor = 0.9. The wavelength of the X-rays is (λ = 1.5406 Å). β is the width (full-width at half-maximum) of the X-ray diffraction peak in radians. θ is the Bragg angle.

The average crystallite size reduced to 5.95 nm for the 0.1% CNT, 6.43 nm (0.5% CNT), 6.35 nm (1% CNT), 8.61 nm (2% CNT), and 7.25 nm (3% CNT). This decrease in crystallite size can be attributed to strains and micro-structural modification corresponding to the CNTs. Addition of CNTs can lead to an interface mismatch due to the difference in atomic radii and bonding with magnesium and carbon species, which hamper the coherent growth of the crystallites and introduce tensile lattice strain [37]. Such results have been observed elsewhere in oxide-type nanocomposite materials, where the lattice distortion, defect creation, and grain size reduction occur after CNT doping [38].

MgO-doped CNTs show significant changes in the structural parameters. The substantial increment in the lattice parameter up to ~ 4.77 Å is an interesting feature in the doped samples. This increase in the lattice constant implies that adding CNTs in the MgO matrix imparts tensile lattice strain. The rise in strain could be due to a mismatch in the atomic radii of Mg and inserted carbon species, and mechanical and interfacial interactions at the MgO/CNT interfaces [37].

Besides the lattice expansion, other diffraction peaks were found in the CNT-doped samples. A strong peak was observed at 2θ ≈ 50.5°, the (012) plane of CNTs, demonstrating their presence in the

CC BY

composite structure. This finding is consistent with earlier findings, where clear CNT-related peaks were only observed after successful incorporation into ceramic or oxide matrices [39].

A second prominent peak was identified at around two θ ≈ 17.8° that did not coincide with known reflections of MgO or CNTs. This unknown peak could be attributed to the generation of an intermediating phase, structural defects, or interfacial compounds, which could be the reactions between MgO and CNTs during synthesis. Such behaviour has been observed previously in literature where, under high-temperature synthesis and dopant inclusion, one gets complex interactions and defect-induced phases [40,41].

UV–Visible Spectroscopy

The optical properties of MgO NPs were studied using UV–Vis absorption spectroscopy over the wavelength range of 200 to 1100 nm, as shown in Fig. 1. The results showed high absorbance at short wavelengths (<300 nm), indicating significant

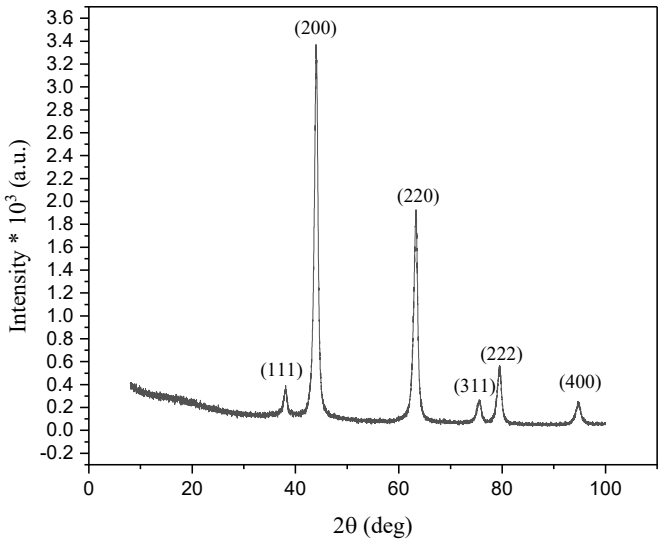


Fig. 1. XRD pattern of pure MgO NPs.

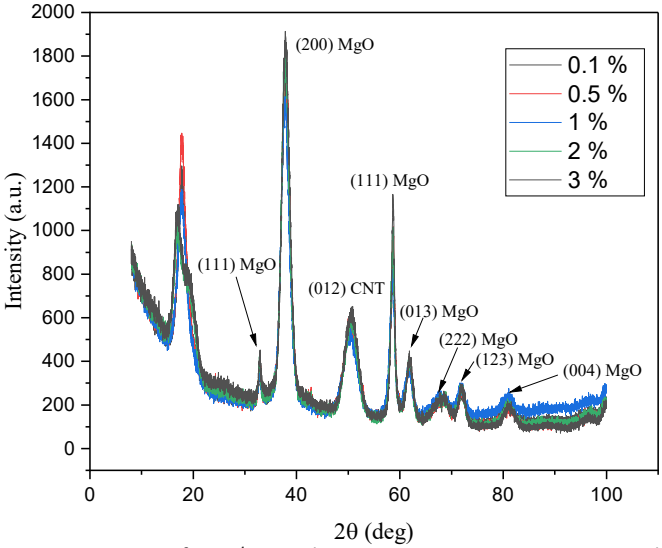


Fig. 2. XRD pattern of MgO/CNT with concentrations 0.1%,0.5%,1%,2%, and 3%.

CC BY

absorption in the ultraviolet region, characteristic of MO-NPs with a wide band gap. A sharp decline in absorbance was observed after the peak, followed by stabilization at lower levels across longer wavelengths, reflecting the insulating nature of MgO. This spectral behavior suggests the presence of a direct electronic transition and confirms the material's broad band gap.

To calculate the optical band gap, the Tauc equation was used, which describes the relationship between the absorption coefficient and the photon energy:

$$\alpha = A(hv - Eg)^{1/2}/hv \quad (2)$$

where α, E_g, and A stand for the absorption coefficient, band gap, and constant, respectively [42]. The optical band gap energy of MgO NPs was found to be 4.05 eV (see Fig. 4), aligning with values documented in prior research [43,44]. The findings demonstrate that MgO functions as a semiconductor with a broad and direct band gap. The band gap of bulk MgO is approximately 7.65 eV. The diminished nanoparticle value is ascribed to the quantum confinement effect caused by the decreased particle size at the nanoscale.

The concentration of CNTs demonstrates nonlinear behavior. We found from Fig. 4 that at low amounts of 0.1% and 0.5%, the band gap was always measured at 4.00 eV, indicating that these small amounts of CNTs were insufficient to cause important changes in the structure or electronics of the MgO NPs. The interaction between CNTs and MgO NPs at these levels seems constrained, with minimal influence on the energy levels. At 1%, a small increase in the band gap to 4.03 eV was observed, likely due to minor improvements in the spread of CNTs, which led to a slight reduction in structural defects. The highest band gap value of 3.94 eV was found at 2%, due to the even spread of CNTs and the prevention of particle clumping. These actions led to a decrease in crystallite size, improving the quantum confinement effect and reinforcing the chemical interaction between MgO NPs and CNTs. This concentration is deemed ideal for attaining improved optical characteristics.

On the other hand, at 3%, the high CNT concentration caused clumping and more structural problems, creating extra energy levels in the band gap and significantly dropping to 3.86 eV. The findings indicate that adjusting the CNT concentration provides an effective method for altering the band gap of MgO/CNT nanocomposites, thereby improving their

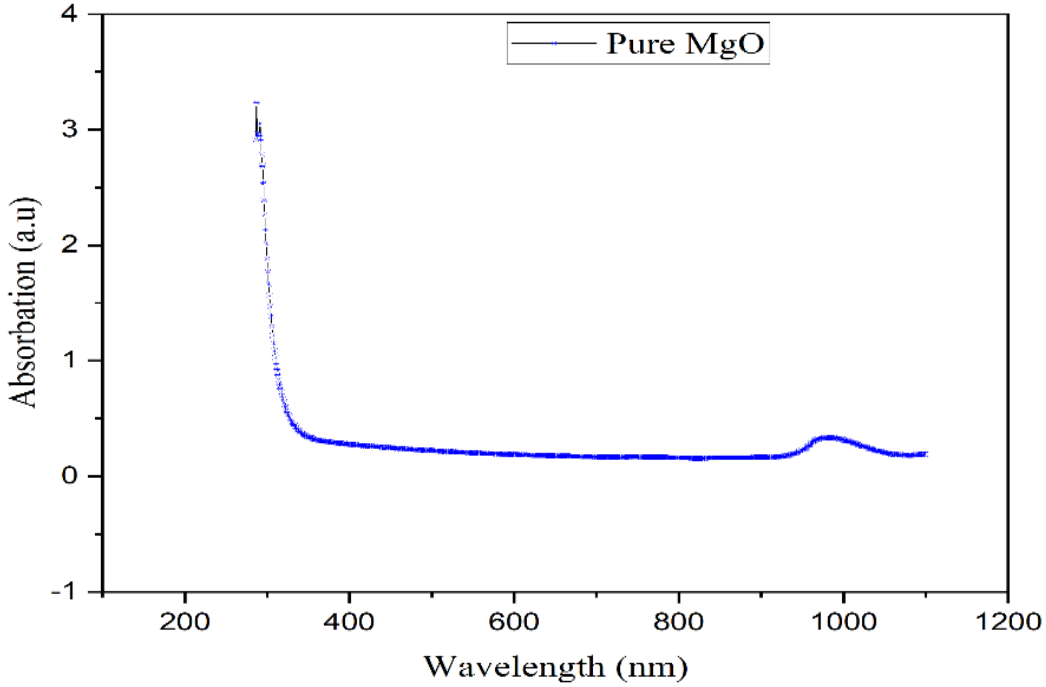


Fig. 3. Absorbance spectra of MgO NPs.

CC BY

applicability in optoelectronics, photocatalysis, and solar energy conversion.

Morphological Studies

The morphology and nanostructure of pure MgO NPs and MgO/CNTs nanocomposites are considerably influenced by the selection of precursors, the regulation of the synthesis processes, and the post-treatment techniques. When CNTs are combined with MgO, it makes the NPs more robust and also enhances their electronic characteristics so that it is better used for advanced applications, including electronics, catalysis, and sensing [45,46].

The field emission scanning electron microscopy (FESEM) images indicated that the

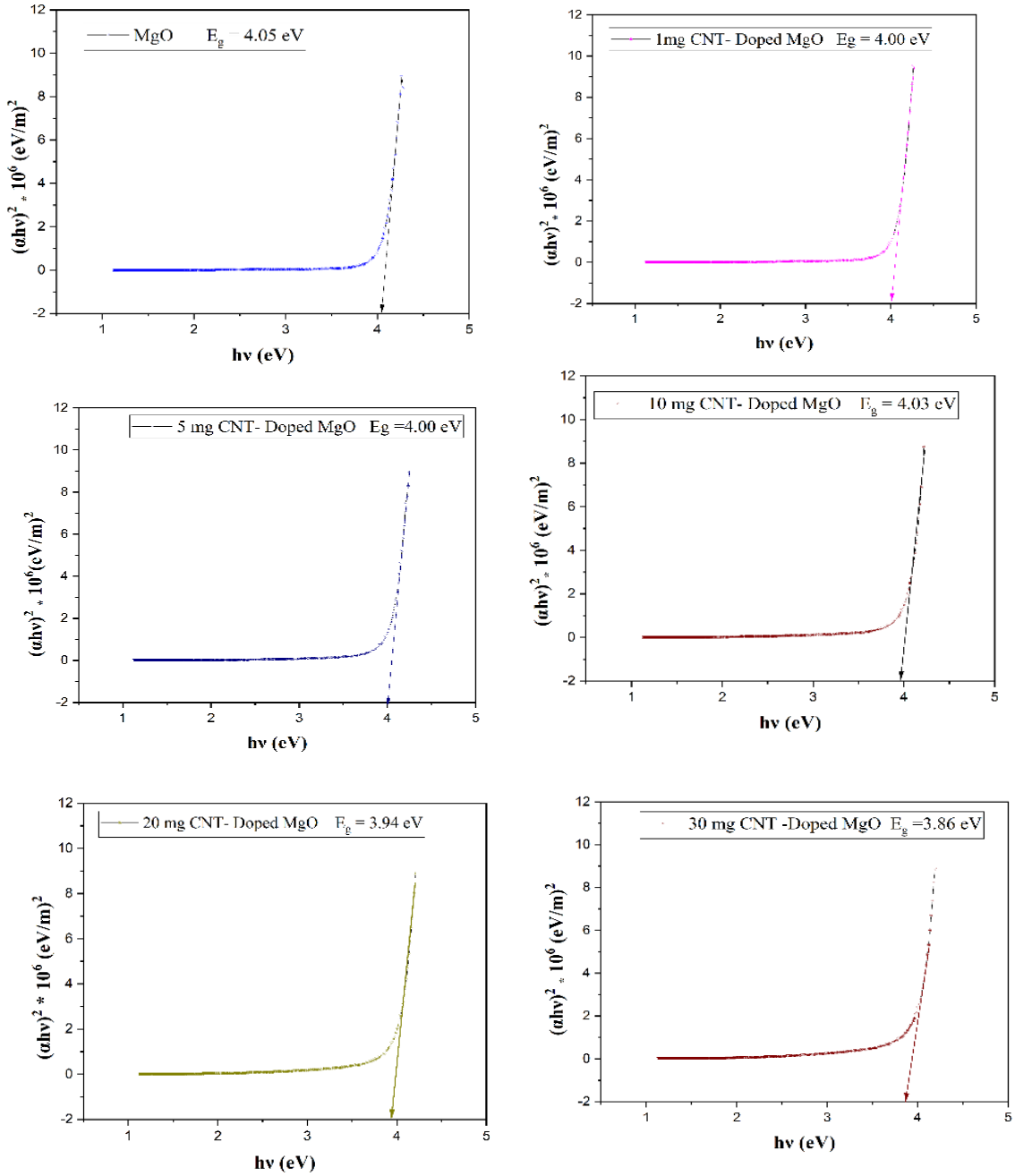


Fig. 4. The determination of the optical band gap energy for MgO doped with CNTs.

CC BY

particle size of pure MgO NPs, Fig. 5a, ranged from 48 to 76 nm, with an average size of 12.2 nm. The MgO NPs exhibited a sponge-like morphology with porous surfaces, the rough properties of these new particles, which slightly agglomerated due to interparticle attractive forces, and their irregular shapes increased their specific surface areas, suggesting their potential use in catalysis, adsorption, and environmental technologies. The presence of CNTs at different concentrations caused marked morphology changes. Fig. 5b at 0.1% CNT, the MgO NPs had significantly larger sizes, moderate agglomeration, irregular shapes, and rugged surfaces, and it was difficult to observe CNTs, which suggested the poor dispersion or weak interaction of MgO NPs and CNTs. Raising

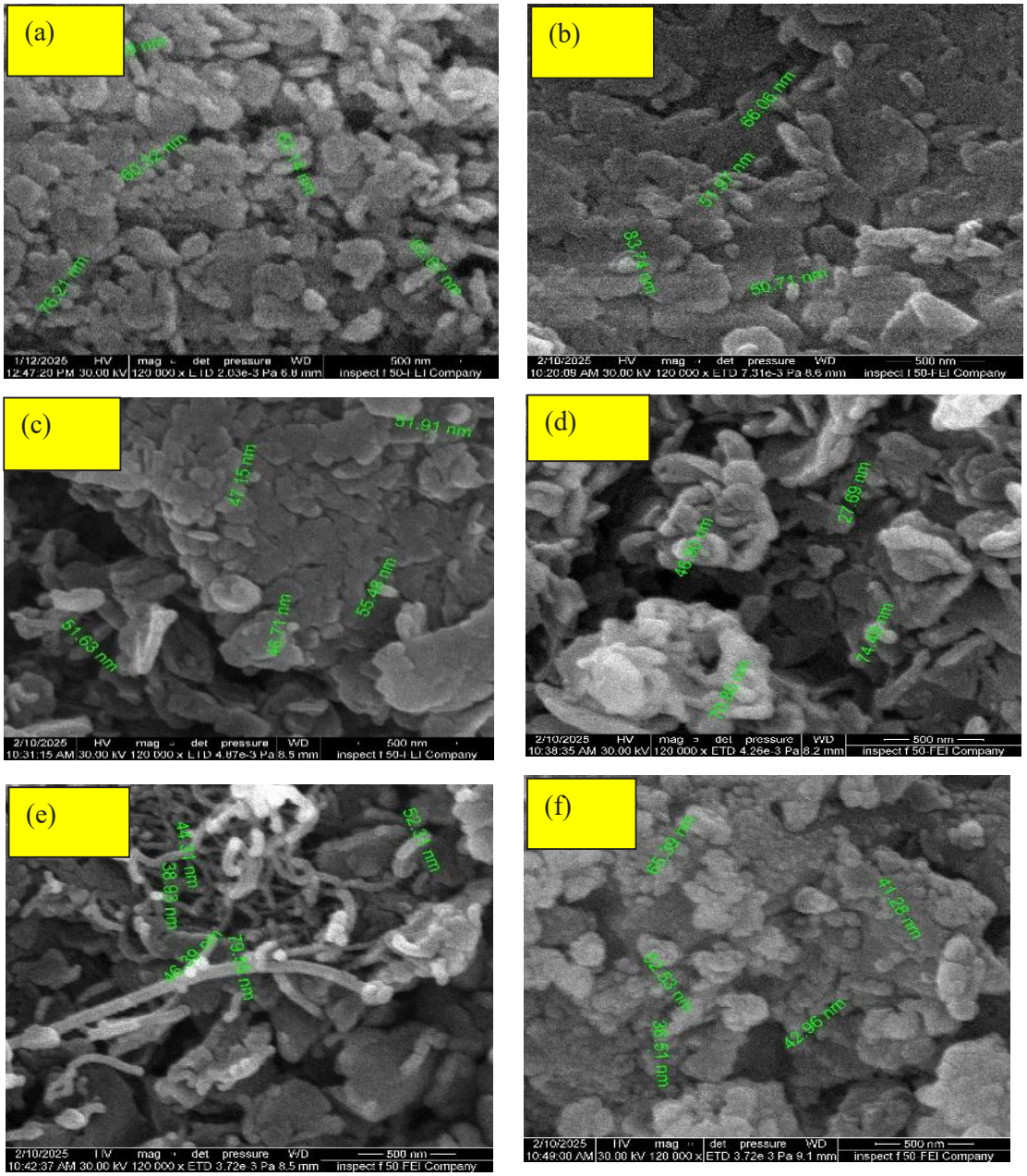


Fig. 5. FESEM images of (a) pure magnesium oxide (MgO), (b) MgO with 0.1 % carbon nanotubes (CNTs), (c) MgO with 0.5 % CNTs, (d) MgO with 1 % CNTs, (e) MgO with 2 % CNTs, and (f) MgO with 3 % CNTs.

the concentrations to 0.5% was responsible for the formation of CNTs at the junctions between particles, which led to partial dissociation of the MgO particles, in agreement with a slight decrease in particle size and a considerable decrease in the particle size distribution and particle shape disorientation. At 1% CNT, facilitating the formation of a more transparent and connected CNT network between MgO NPs, leading to decreased absorption due to clustering. The MgO NPs seemed smaller and more uniform; however, the surface turned rough as CNTs and MgO NPs were intensified by interaction. A further elevation of the content to 2% CNT led to a homogeneously covered network, CNTs interposed between and covering MgO NPs, thus resulting in a greatly enhanced dispersion, a reduced agglomeration of the MgO NPs, and an increase in the specific surface area. Conversely, at 3% CNT, the individual CNTs could not be identified in the FESEM image, even though the CNT content was higher. the CNTs were likely agglomerated or completely covered with the MgO NPs during calcination, however, CNTs were very difficult to observe. Although the size of MgO NPs remained relatively small, a re-aggregation of the particles in the region covering hidden CNT regions was observed, indicating that an overloading of CNTs might have a detrimental effect on the nanocomposite shape.

Antibacterial activity

The antibacterial activity of pure MgO NPs and with CNT doping on Serratia and Streptococcus was determined by agar well diffusion process as shown in Figs. 6 to 11. The test was carried out at nanoparticle levels of 128, 256, 512, and 1024 µg/ml. Bacterial isolates were each grown in nutrient broth at 37°C for 18-24 hours. After incubation, 0.1 mL of each bacterial suspension was spread on the nutrient agar plate and incubated at 37°C for 24 h. A single bacterial colony was transferred onto a test tube containing 5 mL of normal saline, preparing a cloudy bacterial paste resembling the standard turbidity solution, which is approximately 1.5×10^8 CFU/mL. A sterile cotton swab was used to streak the bacterial suspension evenly on Mueller-Hinton agar and incubated for 10 min. The agar was punctured with 5-mm diameter wells (5 wells per plate). Following this, the agar discs were removed, and 50 µL of each pure and crude EPS was added to each well using a micropipette, with the middle well containing deionized water (DW) as a control. The diameter of inhibitory zones was measured after incubating the plates at 37°C for 18h. We chose the bacteria Serratia and Streptococcus to see how well pure MgO and

Table 1. Concentrations and inhibition zone diameters in millimeters (mm) of MgO NPs doped with various levels of CNTs against *Streptococcus* bacteria.

CNT Doping level	Inhibition Zone Diameters (mm)				
	2048 µg/ml	1024 µg/ml	512 µg/ml	256 µg/ml	128 µg/ml
0% (pure MgO)	--	25	23	18	25
0.1%	20	24	5	10	12
0.5%	25	26	18	4	5
1%	25	25	22	16	6
2%	26	24	22	22	14
3%	29	27	26	23	22

Table 2. Concentrations and inhibition zone diameters in millimeters (mm) of MgO NPs doped with various levels of CNTs against *Serratia* bacteria.

CNT Doping level	Inhibition Zone Diameters (mm)				
	2048 µg/ml	1024 µg/ml	512 µg/ml	256 µg/ml	128 µg/ml
0% (pure MgO)	--	27	25	28	24
0.1%	15	15	18	10	8
0.5%	25	18	15	15	12
1%	25	20	18	12	8
2%	28	26	22	23	15
3%	28	27	25	25	22

CC BY

MgO with carbon nanotubes work against these microbes.

The antibacterial activity of MgO NPs with MgO/ CNT was demonstrated on gram-positive Streptococcus, commonly found in the mouth, and gram-negative Serratia, known to be present in the respiratory system [47]. MgO NPs were highly effective for the eradication of gram-positive strains of bacteria, though less effective against gram-negative bacteria [48,49]. CNTs added to MgO NPs vastly improved their ability to repel gram-negative bacteria [49]. The varying areas at which bacteria can no longer grow are a result of different sensitivities of the various kinds

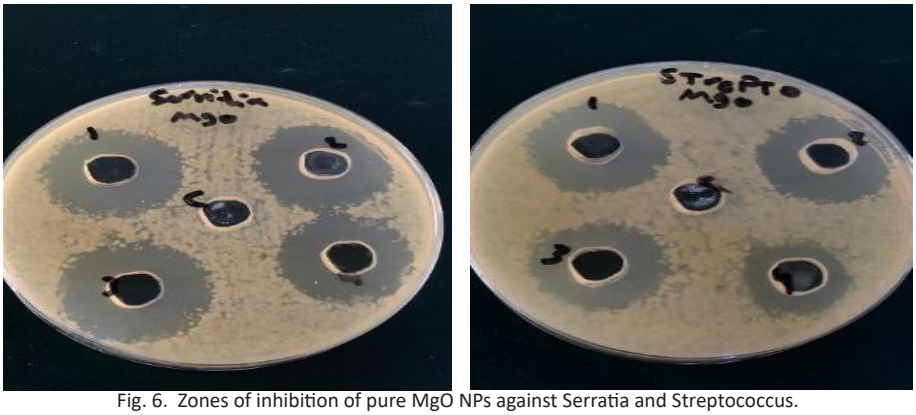


Fig. 6. Zones of inhibition of pure MgO NPs against Serratia and Streptococcus.

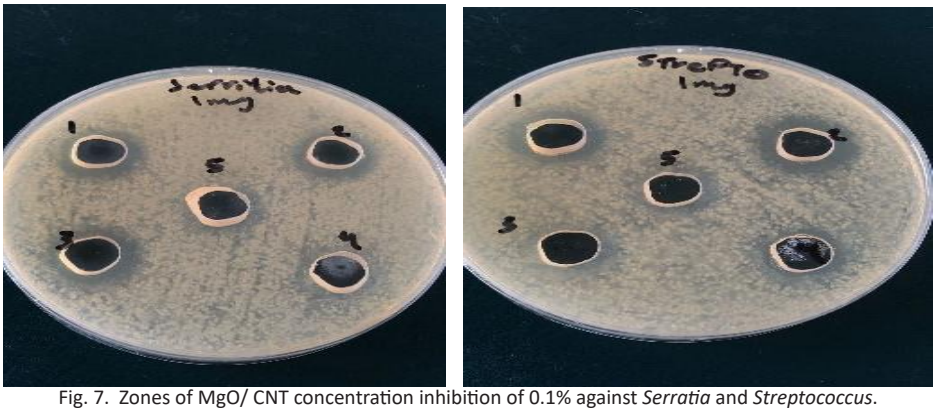


Fig. 7. Zones of MgO/ CNT concentration inhibition of 0.1% against *Serratia* and *Streptococcus*.

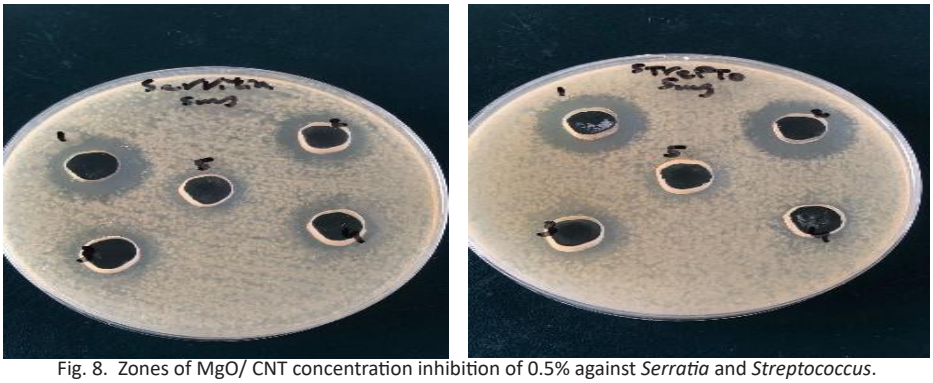


Fig. 8. Zones of MgO/ CNT concentration inhibition of 0.5% against *Serratia* and *Streptococcus*.

CC BY

of bacteria to MgO NPs and MgO/ CNTs [50], has a thick cell wall composed of the peptidoglycan layer, such that there are many layers of this substance in the body of the bacterium, and does not have an outer membrane, and is therefore more easily destroyed by antibacterial drugs. Gram-negative bacteria, however, have a more complex cell wall structure consisting of a cytoplasmic membrane and an outer cell membrane separated by an intermediate layer of peptidoglycan, and are consequently more resistant to antibacterial medicines [51-53].

Tables 1 and 2 show the concentrations and inhibition zone diameters where both the MgO

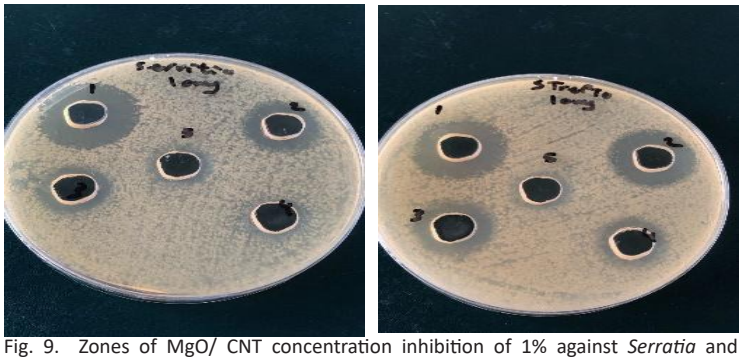


Fig. 9. Zones of MgO/ CNT concentration inhibition of 1% against *Serratia* and *Streptococcus*.

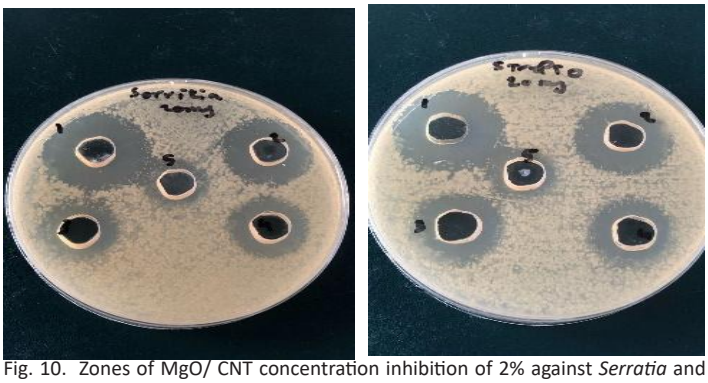


Fig. 10. Zones of MgO/ CNT concentration inhibition of 2% against *Serratia* and *Streptococcus*.

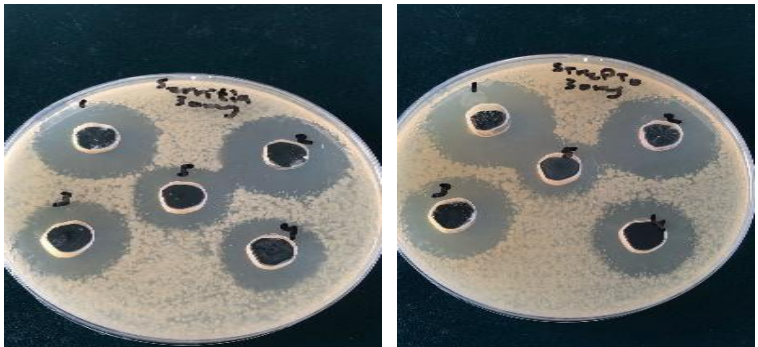


Fig. 11. Zones of MgO/ CNT concentration inhibition of 3% against *Serratia* and *Streptococcus*.

CC BY

NPs and their mixtures with CNT can kill bacteria in different amounts for *Streptococcus* and *Serratia,* respectively. The results showed that using more MgO, whether by itself or with CNTs, led to a larger area where bacteria were killed, making it more effective at eliminating the tested bacteria. Strain-dependent differences occurred between organisms, as Streptococcus sometimes responded better than Serratia. Carbon nanotube (CNT) addition increased the antimicrobial activity at some concentrations, especially at 3%.

CONCLUSION

The sol-gel process was successfully used to synthesize MgO/CNTs nanocomposites. The experimental results indicated that adding CNTs to MgO resulted in significant improvements in the structure, optical properties, and strength of the new composite. The X-ray diffraction (XRD) showed that the crystal size decreased significantly when CNTs were doped in the MgO particles, which explained the changes in the crystal structure and offered a much higher surface area of the MgO nanoparticles for reaction. The structural evolution of CNTs played an important role in the formation of the crystal for magnesium oxide. The contact between CNTs and magnesium resulted in lattice parameter expansion and indicated that the lattice was stretched due to the interaction and atomic size difference of the materials. The UV-Vis spectroscopy results showed that the optical band gap value was reduced from 4.05 eV for the pure MgO to 3.86 eV at 3% CNT co-doping into the MgO nanoparticles. The interaction between the materials can be seen as a cause of the decrease in the band gap and contributes to the better optical properties of the material, making it eligible as a material in, for instance, solar energy conversion and in optoelectronics. Biological tests revealed that the obtained MgO/CNT nanocomposites possessed a high antibacterial activity against both Serratia and Streptococcus bacteria. The inhibitory zones were strongest at 3% CNT as the highest. This result implies that the nanocomposite is highly antibacterial against various bacteria, and it could be used in water purification and surface disinfection in both environmental and medical applications.

ACKNOWLEDGEMENT

The author would like to acknowledge the provision of instruments and necessary materials by Department of Physics, College of Science, University of Babylon. Special thanks go to **HT Sim** for the helping in complete the work.

CONFLICT OF INTEREST

The authors declare that there is no conflict of interests regarding the publication of this manuscript.

REFERENCES

1. Luo J, Yang X, Xue Y, Yang C, Yang Z, Tusiime R, et al. Simultaneous optimization of the thermal conductivity and mechanical properties of epoxy resin composites through PES and AgNP functionalized BNs. Composites Part B: Engineering. 2023;248:110373.
2. Zhan H, Chen YW, Shi QQ, Zhang Y, Mo RW, Wang JN. Highly aligned and densified carbon nanotube films with superior thermal conductivity and mechanical strength. Carbon. 2022;186:205-214.
3. Kubiak JM, Li B, Suazo M, Macfarlane RJ. Polymer Grafted Nanoparticle Composites with Enhanced Thermal and Mechanical Properties. ACS Applied Materials and Interfaces. 2022;14(18):21535-21543.
4. Sun B, Hu P, Ji X, Fan M, Zhou L, Guo M, et al. Excellent Stability in Polyetherimide/SiO_2 Nanocomposites with Ultrahigh Energy Density and Discharge Efficiency at High Temperature. Small. 2022;18(28).
5. Ahmad S, Ali K, Ashraf M, Khalifa HAE-W, Aziz ElSeabee FA, Tag El Din ESM. Analysis of pure nanofluid (GO/engine oil) and hybrid nanofluid (GO–Fe_3O_4/engine oil): Novel thermal and magnetic features. Nanotechnology Reviews. 2022;11(1):2903-2915.
6. Wang X, Liu K, Su Y, Wang X, Cao H, Hua A, et al. Synergistic enhancing effect of tungsten-copper coated graphite flakes and aluminum nitride nanoparticles on microstructure, mechanical and thermal properties of copper matrix composites. Materials Science and Engineering: A. 2022;857:143987.
7. Sobhy M. Hygrothermal deformation of orthotropic nanoplates based on the state-space concept. Composites Part B: Engineering. 2015;79:224-235.
8. Akbari A, Amini M, Tarassoli A, Eftekhari-Sis B, Ghasemian N, Jabbari E. Transition metal oxide nanoparticles as efficient catalysts in oxidation reactions. Nano-Structures and Nano-Objects. 2018;14:19-48.
9. Nikolic MV, Vasiljevic ZZ, Auger S, Vidic J. Metal oxide nanoparticles for safe active and intelligent food packaging. Trends in Food Science and Technology. 2021;116:655-668.
10. Murthy S, Effiong P, Fei CC. Metal oxide nanoparticles in biomedical applications. Metal Oxide Powder Technologies: Elsevier; 2020. p. 233-251. http://dx.doi.org/10.1016/b978-0-12-817505-7.00011-7
11. Nikolova MP, Chavali MS. Metal Oxide Nanoparticles as Biomedical Materials. Biomimetics. 2020;5(2):27.
12. Abinaya S, Kavitha HP, Prakash M, Muthukrishnaraj A. Green synthesis of magnesium oxide nanoparticles and its applications: A review. Sustainable Chemistry and Pharmacy. 2021;19:100368.
13. Hornak J, Trnka P, Kadlec P, Michal O, Mentlík V, Šutta P, et al. Magnesium Oxide Nanoparticles: Dielectric Properties, Surface Functionalization and Improvement of Epoxy-

Based Composites Insulating Properties. Nanomaterials. 2018;8(6):381.
14. Akhtar MW, Kim JS, Memon MA, Khan MY, Baloch MM. Surface modification of magnesium oxide/epoxy composites with significantly improved mechanical and thermal properties. Journal of Materials Science: Materials in Electronics. 2021;32(11):15307-15316.
15. Nigam A, Saini S, Rai AK, Pawar SJ. Structural, optical, cytotoxicity, and antimicrobial properties of MgO, ZnO and MgO/ZnO nanocomposite for biomedical applications. Ceram Int. 2021;47(14):19515-19525.
16. Hornak J. Synthesis, Properties, and Selected Technical Applications of Magnesium Oxide Nanoparticles: A Review. Int J Mol Sci. 2021;22(23):12752.
17. Chinthala M, Balakrishnan A, Venkataraman P, Manaswini Gowtham V, Polagani RK. Synthesis and applications of nano-MgO and composites for medicine, energy, and environmental remediation: a review. Environ Chem Lett. 2021;19(6):4415-4454.
18. Harris PJF. Carbon nanotube composites. Int Mater Rev. 2004;49(1):31-43.
19. Aqel A, El-Nour KMMA, Ammar RAA, Al-Warthan A. Carbon nanotubes, science and technology part (I) structure, synthesis and characterisation. Arabian Journal of Chemistry. 2012;5(1):1-23.
20. Venkataraman A, Amadi EV, Chen Y, Papadopoulos C. Carbon Nanotube Assembly and Integration for Applications. Nanoscale Research Letters. 2019;14(1).
21. Gupta N, Gupta SM, Sharma SK. Carbon nanotubes: synthesis, properties and engineering applications. Carbon Letters. 2019;29(5):419-447.
22. Seah C-M, Chai S-P, Mohamed AR. Synthesis of aligned carbon nanotubes. Carbon. 2011;49(14):4613-4635.
23. Yan Y, Miao J, Yang Z, Xiao F-X, Yang HB, Liu B, et al. Carbon nanotube catalysts: recent advances in synthesis, characterization and applications. Chem Soc Rev. 2015;44(10):3295-3346.
24. Burakova EA, Dyachkova TP, Rukhov AV, Tugolukov EN, Galunin EV, Tkachev AG, et al. Novel and economic method of carbon nanotubes synthesis on a nickel magnesium oxide catalyst using microwave radiation. J Mol Liq. 2018;253:340-346.
25. Dubey R, Dutta D, Sarkar A, Chattopadhyay P. Functionalized carbon nanotubes: synthesis, properties and applications in water purification, drug delivery, and material and biomedical sciences. Nanoscale Advances. 2021;3(20):5722-5744.
26. Raphey VR, Henna TK, Nivitha KP, Mufeedha P, Sabu C, Pramod K. Advanced biomedical applications of carbon nanotube. Materials Science and Engineering: C. 2019;100:616-630.
27. Bindhu MR, Umadevi M, Kavin Micheal M, Arasu MV, Abdullah Al-Dhabi N. Structural, morphological and optical properties of MgO nanoparticles for antibacterial applications. Mater Lett. 2016;166:19-22.
28. He Y, Ingudam S, Reed S, Gehring A, Strobaugh TP, Irwin P. Study on the mechanism of antibacterial action of magnesium oxide nanoparticles against foodborne pathogens. Journal of Nanobiotechnology. 2016;14(1).
29. Alnahari H, Al-Hammadi AH, Al-Sharabi A, Alnehia A, Al-Odayni A-B. Structural, morphological, optical, and antibacterial properties of $CuO–Fe_2O_3–MgO–CuFe_2O_4$ nanocomposite synthesized via auto-combustion route. Journal of Materials Science: Materials in Electronics. 2023;34(7).
30. Wahab R, Ansari SG, Dar MA, Kim YS, Shin HS. Synthesis of Magnesium Oxide Nanoparticles by Sol-Gel Process. Mater Sci Forum. 2007;558-559:983-986.
31. Yin Z, Li X, Li S, Shi W, Wang A, Gao J, et al. Investigation of fuel type on the microstructure and antibacterial activity of Li-doped MgO nanoparticles. Ceram Int. 2024;50(1):1633-1642.
32. Sim HT, Gençaslan M, Merdan M. Synthesis of MgO nanoparticles via the sol-gel method for antibacterial applications, investigation of optical properties and comparison with commercial MgO. Discover Applied Sciences. 2024;6(11).
33. Barzegar M, Ahmadvand D, Sabouri Z, Darroudi M. Phytoextract-mediated synthesis of magnesium oxide nanoparticles using Caccinia macranthera extract and examination of their photocatalytic and anticancer effects. Mater Res Bull. 2024;169:112514.
34. Prabhu YT, Venkateswara Rao K, Siva Kumari B, Pavani T. Decoration of magnesium oxide nanoparticles on O-MWCNTs and its antibacterial studies. Rendiconti Lincei. 2015;26(3):263-270.
35. Rani N, Chahal S, Chauhan AS, Kumar P, Shukla R, Singh SK. X-ray Analysis of MgO Nanoparticles by Modified Scherer's Williamson-Hall and Size-Strain Method. Materials Today: Proceedings. 2019;12:543-548.
36. Endla P. Structure, morphology, and luminescence properties of sol–gel-synthesized pure and cobalt-doped MgO nanoparticles. Ionics. 2024;30(11):7653-7663.
37. Endla P. Exploring the enhanced mechanical and magnetic properties of nickel-doped magnesium oxide nanoparticles. Journal of Materials Science: Materials in Electronics. 2024;35(16).
38. Siddiqui H, Parra MR, Qureshi MS, Malik MM, Haque FZ. Studies of structural, optical, and electrical properties associated with defects in sodium-doped copper oxide (CuO/Na) nanostructures. Journal of Materials Science. 2018;53(12):8826-8843.
39. Ali ME, Alfaki AA, Mohammed AS, Abuelhassan HH, Qurtam AA, Haroun KM, et al. Synthesis and characterization of carbon nanotubes incorporated with MgO nanoparticles. Journal of Ovonic Research. 2021;17(5):429-435.
40. Cao Y, Jiao Q, Zhao Y, Dong Y. Decorating Mg/Fe oxide nanotubes with nitrogen-doped carbon nanotubes. J Alloys Compd. 2011;509(38):9372-9376.
41. Ning G, Xu C, Zhu X, Zhang R, Qian W, Wei F, et al. MgO-catalyzed growth of N-doped wrinkled carbon nanotubes. Carbon. 2013;56:38-44.
42. Singh N, Singh PK, Shukla A, Singh S, Tandon P. Synthesis and Characterization of Nanostructured Magnesium Oxide: Insight from Solid-State Density Functional Theory Calculations. Journal of Inorganic and Organometallic Polymers and Materials. 2016;26(6):1413-1420.
43. Badar N, Chayed NF, Roshidah R, Kamarudin N, Kamarulzaman N. Band Gap Energies of Magnesium Oxide Nanomaterials Synthesized by the Sol-Gel Method. Advanced Materials Research. 2012;545:157-160.
44. Yousefi S, Ghasemi B, Tajally M, Asghari A. Optical properties of MgO and $Mg(OH)_2$ nanostructures synthesized by a chemical precipitation method using impure brine. J Alloys Compd. 2017;711:521-529.
45. Sutradhar N, Sinhamahapatra A, Pahari SK, Pal P, Bajaj HC, Mukhopadhyay I, et al. Controlled Synthesis of Different Morphologies of MgO and Their Use as Solid Base Catalysts. The Journal of Physical Chemistry C. 2011;115(25):12308-

CC BY

12316.
46. Mohana P, Isacfranklin M, Yuvakkumar R, Ravi G, Kungumadevi L, Arunmetha S, et al. Facile Synthesis of Ni-MgO/CNT Nanocomposite for Hydrogen Evolution Reaction. Nanomaterials. 2024;14(3):280.
47. Niazvand F, Sharifianjazi F, Esmaeilkhanian A, Ahmadi E, Moradigharibvand N, Rabiee N, et al. Sol-gel derived bioactive glasses containing boron and strontium: Bioactivity, biocompatibility, and antibacterial properties. Journal of Non-Crystalline Solids. 2024;631:122909.
48. Nguyen N-YT, Grelling N, Wetteland CL, Rosario R, Liu H. Antimicrobial Activities and Mechanisms of Magnesium Oxide Nanoparticles (nMgO) against Pathogenic Bacteria, Yeasts, and Biofilms. Sci Rep. 2018;8(1).
49. Rodríguez-Hernández A-P, Vega-Jiménez AL, Vázquez-Olmos AR, Ortega-Maldonado M, Ximenez-Fyvie L-A. Antibacterial Properties In Vitro of Magnesium Oxide Nanoparticles for Dental Applications. Nanomaterials. 2023;13(3):502.
50. Bhattacharya P, Dey A, Neogi S. An insight into the mechanism of antibacterial activity by magnesium oxide nanoparticles. Journal of Materials Chemistry B. 2021;9(26):5329-5339.
51. Vollmer W, Höltje J-V. The Architecture of the Murein (Peptidoglycan) in Gram-Negative Bacteria: Vertical Scaffold or Horizontal Layer(s)? J Bacteriol. 2004;186(18):5978-5987.
52. Kim SJ, Chang J, Singh M. Peptidoglycan architecture of Gram-positive bacteria by solid-state NMR. Biochim Biophys Acta. 2015;1848(1):350-362.
53. Vancomycin-Polyguanidino Dendrimer Conjugates Inhibit Growth of Antibiotic-Resistant Gram-Positive and Gram-Negative Bacteria and Eradicate Biofilm-Associated S.aureus. American Chemical Society (ACS). http://dx.doi.org/10.1021/acsinfecdis.3c00168.s001

CC BY